Journal of
Micro/Nanolithography,
MEMS, and MOEMS

Nanolithography.SPIEDigitalLibrary.org

Photochemical conversion of tin-oxo cage compounds studied using hard x-ray photoelectron spectroscopy

Yu Zhang
Jarich Haitjema
Xiaomeng Liu
Fredrik Johansson
Andreas Lindblad
Sonia Castellanos
Niklas Ottosson
Albert M. Brouwer

SPIE.

Yu Zhang, Jarich Haitjema, Xiaomeng Liu, Fredrik Johansson, Andreas Lindblad, Sonia Castellanos, Niklas Ottosson, Albert M. Brouwer, "Photochemical conversion of tin-oxo cage compounds studied using hard x-ray photoelectron spectroscopy," *J. Micro/Nanolith. MEMS MOEMS* **16**(2), 023510 (2017), doi: 10.1117/1.JMM.16.2.023510.

Photochemical conversion of tin-oxo cage compounds studied using hard x-ray photoelectron spectroscopy

Yu Zhang,[a] Jarich Haitjema,[a] Xiaomeng Liu,[a] Fredrik Johansson,[b] Andreas Lindblad,[b] Sonia Castellanos,[a] Niklas Ottosson,[a,c] and Albert M. Brouwer[a,d,*]
[a]Advanced Research Center for Nanolithography, Amsterdam, The Netherlands
[b]Uppsala University, Division of Molecular and Condensed Matter Physics, Department of Physics and Astronomy, Ångströmlaboratoriet, Uppsala, Sweden
[c]AMOLF, Amsterdam, The Netherlands
[d]University of Amsterdam, van 't Hoff Institute for Molecular Sciences, Faculty of Science, Amsterdam, The Netherlands

Abstract. Molecular inorganic materials are currently considered photoresists for extreme ultraviolet lithography (EUVL). Their high EUV absorption cross section and small building block size potentially allow high sensitivity and resolution as well as low line-edge roughness. The photochemical reaction mechanisms that allow these kinds of materials to function as photoresists, however, are still poorly understood. We discuss photochemical reactions upon deep UV (DUV) irradiation of a model negative-tone EUV photoresist material, namely the well-defined molecular tin-oxo cage compound $[(SnBu)_{12}O_{14}(OH)_6](OH)_2$, which is spin-coated to thin layers of 20 nm. The core electronic structures (Sn 3d, O 1s, and C 1s) of unexposed and DUV exposed films were then investigated using synchrotron radiation-based hard x-ray photoelectron spectroscopy. Different chemical oxidation states and concentrations of atoms and atom types in the unexposed and exposed films were found. We observed that the exposure in a nitrogen atmosphere prevented the oxidation but still led to carbon loss, albeit with a smaller conversion. Finally, a mechanistic hypothesis for the basic DUV photoreactions in molecular tin-oxo cages is proposed. [DOI: 10.1117/1.JMM.16.2.023510]

Keywords: inorganic photoresist; tin-oxo cages; hard x-ray photoelectron spectroscopy; photochemical mechanism; deep UV.

Paper 17046P received Apr. 10, 2017; accepted for publication Jun. 2, 2017; published online Jun. 22, 2017.

1 Introduction

Metal-containing hybrid inorganic materials are considered promising candidates as photoresists in high volume semiconductor manufacturing using extreme ultraviolet lithography (EUVL), ever since these materials were introduced in the past years.[1–5] Photoresists based on HfO_2 and ZrO_2 nanoparticles were synthesized and shown to form patterns in EUVL by Ober's group.[1–3] Tin-oxo cages,[6] palladium complexes,[7] organotin compounds,[8] and other molecular compounds have further been explored as EUV photoresist by Brainard's group. Recently, Inpria introduced Sn-based hybrid photoresists.[5] Compared with traditional organic chemically amplified photoresists (CARs), some of these inorganic photoresists show higher sensitivity,[2,4,9,10] can form thinner layers, have higher etching resistance,[9] and potentially yield both lower line-edge roughness and higher resolution due to the smaller building blocks.[11–13] Such findings have shown the great potential for inorganic materials to be used as EUV photoresist. CARs have now been used and optimized for many years, first for deep UV (DUV) and more recently for EUV, and their critical photochemical reactions are generally well understood.[14] In contrast, the photoreaction mechanisms in the inorganic photoresist have not been thoroughly investigated yet. To further improve the performance of the inorganic photoresists, systematic studies of the key photoreaction mechanisms in the photoresist are necessary.

In this contribution, we study the structure and photochemistry in spin-coated layers of the tin-oxo cage compound $[(SnBu)_{12}O_{14}(OH)_6](OH)_2$, which can be seen as an ideal model system of inorganic nanoscale photoresists, given its well-defined metal-oxo core structure with surrounding *n*-butyl organic ligands and hydroxide counterions; see Fig. 1. To synthesize the compound, we followed the route in Ref. 15. The molecule contains Sn atoms with high EUV photon absorption,[10,16,17] and it has been demonstrated to work as an EUV photoresist.[6,8] Despite the relatively simple structure of this molecular system, few spectroscopic methods are suitable to study the details of the photochemical reactions occurring in thin films, both due to limited sensitivity and limited chemical contrast. For example, UV-absorption spectra contain little structural information, while vibrational spectra (Raman or IR absorption) of thin films are close to their sensitivity limits, and, in the case of the tin cages, give limited information due to the absence of characteristic vibrational marker bands. Here, we apply hard x-ray photoelectron spectroscopy (HAXPES) with tunable high photon energies from synchrotron sources, typically ranging from 1.7 to 10 keV. The detection limit is extremely low, and core-level photoemission naturally gives rise to elemental sensitivity because each element emits electrons from core levels in completely separated and well-defined energy ranges. The known relative emission efficiencies for different core levels allow quantitative analysis of chemical composition. The chemical shifts in the binding energies of atoms in chemically different bonding environments make the method sensitive to chemical structure.[18]

*Address all correspondence to: Albert M. Brouwer, E-mail: f.brouwer@arcnl.nl

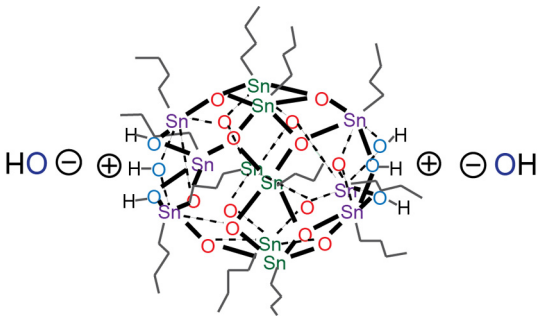

Fig. 1 Molecular structure of the $[(SnBu)_{12}O_{14}(OH)_6](OH)_2$ tin-oxo cage compound.

Finally, the high photon energy in HAXPES gives the photoemitted electrons high kinetic energy and thus long inelastic mean free paths that allow the probing of molecular layers far below the surface. Thus, the bulk properties of the spin-coated photoresist layer can be accessed before and after exposure.[19]

2 Experimental

2.1 *Materials*

The tin-oxo cage with tosylates as counterions (TinS) was synthesized from butylstannoic acid hydrate and *p*-toluene sulfonic acid monohydrate.[15] Tin-oxo cages with hydroxide as counterions (TinOH) were obtained by mixing a solution of aqueous tetramethylammonium hydroxide with a solution of TinS in isopropanol. TinOH precipitated, and the product was filtered directly. Results of a more extensive series of tin cage compounds will be published elsewhere. Glass coverslips were purchased from Menzel Gläser and cut into 1×1 cm^2.

2.2 *Photoresist Film Preparation*

For photoelectron spectroscopy experiments, it is essential that the substrates are conducting. These were prepared by coating piranha base-cleaned glass coverslips with 2-nm Cr and 18-nm Au layers using a sputter coater (Leica EM ACE 600 Double sputter coater). The tin-oxo cage material was dissolved in toluene to a concentration of 7.5 mg/mL. Solutions were filtered through a 0.25-μm PTFE filter right before spin coating. Thin layers [~20 nm, determined by atomic force microscopy (AFM)] were obtained by spin coating under 2000 rpm for 45 s with a speed of 750 rpm/s on the Cr/Au-coated glass coverslips. The samples were subjected to post-application bake at 90°C for 1 min.

2.3 *Photoresist Exposure*

A YAG-pumped OPA laser (Ekspla NT342B), delivering nanosecond pulses at 225 nm at 10 Hz (2.5 mJ/pulse), was used as the irradiation source. Some samples were exposed under ambient conditions with a dose of 1.3 J/cm^2. The dose was chosen to ensure a substantial chemical conversion in this first study of product formation. The other samples were exposed in an enclosed sample chamber containing dry N_2, to the same dose (i.e., the exposure time was corrected for the losses due to window reflectivity).

2.4 *Characterization*

All samples were characterized using HAXPES at the HIKE end station, located at the KMC-1 bending-magnet beamline at BESSY-II, Helmholtz–Zentrum–Berlin.[20] The photoelectron spectra were collected with a VG Scienta R4000 hemispherical electron energy analyzer, which can analyze electron kinetic energies up to 10 keV. The pressure in the experimental chamber was in the low 10^{-9} mbar range, and the samples were introduced via a load-lock chamber. The photon energy used for measurement was 2005 eV. Variation of the photon energy was done to unambiguously assign features to direct photoionization lines, which show an electron kinetic energy that increases with the incident photon energy, in contrast to Auger transitions that have constant kinetic energy. The total energy resolution of the experiment, with the main contributions coming from the photon bandwidth and the electron analyzer resolution, was estimated to be ~250 meV. Two types of spectra were recorded: (i) overview spectra taken from 0 to 800 eV binding energy (BE) in which all relevant lines were included and (ii) detailed core-level spectra of the Sn 3d, C 1s, and O 1s regions. The overview spectra were used to extract atomic number ratios, whereas the detailed spectra were used to resolve the chemical shifts in the respective elemental region. The x-ray power was ~10 μW/cm^2, which allowed the recording of a spectrum in a few minutes. Radiation damage to the materials was apparent only after ca. 2 h.

3 Result and Discussion

3.1 *Atomic Concentration of Different Samples*

Overview HAXPES spectra of unexposed TinOH thin films, as well as samples exposed to DUV in air and in N_2, are shown in Fig. 2. All the peaks are marked with the electronic state from which the electrons originate. Au 4f peaks, originating from the layer underneath the tin cage layer, are present in the spectra and were used for binding energy calibration; the Au $4f_{7/2}$ binding energy was taken to be 84.00 eV.[21] The tin cage gives rise to clear Sn 3d peaks at ~487 and ~498 eV (5/2 and 3/2 spin-orbit components, respectively), an O 1s peak at ~531 eV, and a C 1s peak at ~284 eV. The peak positions correspond well with those in the literature.[19,22–24]

The atomic ratios of Sn, O, and C atoms inside the three samples are proportional to the area ratios of the peaks in the spectrum and can be extracted with knowledge of the photoionization cross sections.[25] For the unexposed sample, the extracted atomic ratios correspond well within the error bar to the expected chemical composition. For the exposed samples, since the number of Sn atoms is unlikely to change due to exposure, the O 1s and C 1s peak areas are normalized to the Sn peak area, and the atom ratios for these samples are given in Table 1.

As can be seen from Table 1, after the TinOH sample was exposed to DUV in air, the oxygen content was significantly increased while the carbon content was drastically decreased. This suggests that oxidation happens during the exposure, together with Sn—C bond or C—C bond cleavage, causing a loss of volatile carbon-containing species. When the sample was exposed in dry N_2, however, the O content stayed the same; this is because when no oxygen-containing gas-phase species is present, no further oxidation is possible and the

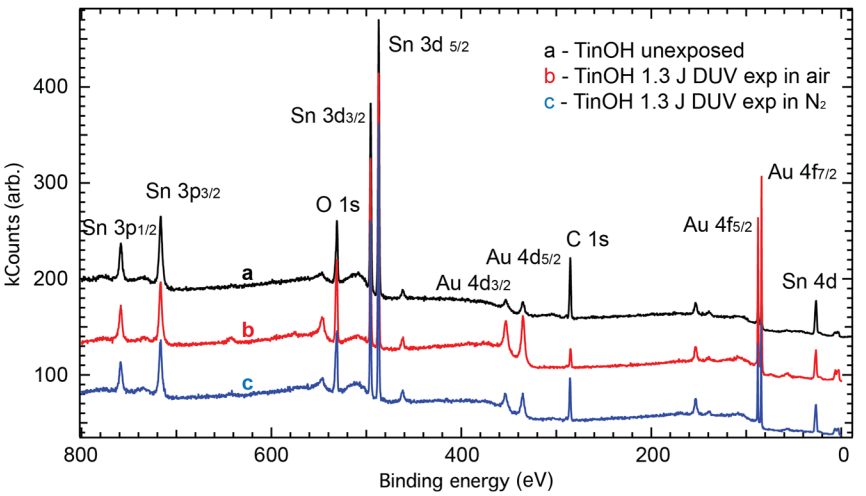

Fig. 2 Overview HAXPES spectrum of TinOH unexposed sample, TinOH DUV-exposed in air, and TinOH DUV-exposed in N_2. (The spectra are displaced vertically to avoid overlapping of the peaks).

Table 1 Atomic ratios of TinOH unexposed sample, TinOH DUV-exposed in air, and TinOH DUV-exposed in N_2.

Atom no.	Sn	O	C
Expected	12	22	48
TinOH_unexposed	12	22 ± 1	48 ± 1
DUV exp air	12	32 ± 1	18 ± 1
DUV exp N_2	12	22 ± 1	36 ± 1

photoinduced outgassing apparently does not cause any further loss of oxygen either. Compared with the carbon loss when TinOH was exposed in air, less C was lost under the same DUV dose.

For the TinOH sample exposed to DUV in air, we can make a crude estimate of the average photochemical quantum yield for breaking of Sn—C bonds based on the loss of carbon of ~63%. Using the measured UV absorbance of the thin film at 225 nm, we find that the absorbed dose is ~0.40 J cm^{-2}. This corresponds to 4.5×10^{17} photons cm^{-2}. These lead to the breaking of 6.7×10^{15} Sn—C bonds per cm^2. The average quantum yield for loss of a butyl group is thus ~1.5%. More accurate quantitative characterization of the photochemical process is needed, but we can already conclude that the carbon loss reaction is not very efficient.

3.2 *Analysis of Sn, O, and C Chemical Shifts*

The high-resolution Sn $3d_{5/2}$ photoelectron spectra of the samples are shown in Fig. 3(a). Small, well-reproducible shifts can be clearly observed, which we interpret as a result of a change of the Sn oxidation state. The dependency of the Sn 3d binding energy on the Sn oxidation state has been well established in the literature.[19] The center of the $Sn3d_{5/2}$ peak after DUV exposure in air is shifted to higher binding energy, indicating that the oxidation state of the Sn atoms has increased. In contrast, the center energy position after DUV exposure in N_2 is shifted to a lower binding energy, indicating a net reduction of Sn atoms.

In Figs. 3(b)–3(d), we show least squares fits to the data using two Voigt line shapes, i.e., each component is a Gaussian convoluted with a Lorentzian function (10%) that accounts for the finite lifetime of the core ionized state. Because there are two kinds of Sn atoms inside the tin-oxo cages (5-coordinated Sn atoms in the center part of molecule, 6-coordinated Sn atoms in the side parts of the molecule facing the counter-ion), two subpeaks were used to model the spectrum of the unexposed sample. Although the photolysis products are probably more complex, we take these peaks to be representative for tin in lower and higher oxidation states, respectively, and use the same peak positions and bandwidths to model the Sn peaks in the exposed samples—leaving only the amplitude as the free parameter. Under these constraints, the spectra in Figs. 3(b)–3(d) were simultaneously fitted for the best global fit describing the full data set.

The results are presented as solid lines in Figs. 3(b)–3(d), together with the data as circles. The peak at 486.7 eV (green) corresponds to the 5-coordinated Sn (low oxidation state, low BE) and the peak at 487.3 eV (purple) to the 6-coordinated Sn (higher oxidation state, high BE). In Fig. 3(b), the intensity of the two peaks is constrained to the 1:1 ratio corresponding to the equal abundance of the two types of tin. After DUV exposure in air, the intensity of the component corresponding to the low oxidation state decreases and the intensity is transferred to the peak of the more highly oxidized Sn component. In contrast, the fitting results from the sample exposed in N_2 indicated that some of the higher oxidation state Sn atoms were converted to a lower oxidation state. The FWHM of the three spectra were 1.58, 1.22, and 1.27 eV, respectively; see Fig. 3(a). The peaks became narrower after exposure because one type of Sn atom became more dominant, but the FWHM values of the underlying components were constant at 1.17 eV.

The O 1s photoelectron spectra are shown in Fig. 4. O 1s peaks from all samples were normalized based on the O atoms ratio obtained from the overview spectra. Similar to the Sn 3d data, Fig. 4(a) shows the O 1s spectra with a common scale on the ordinate axis, whereas Figs. 4(b)–4(d) show

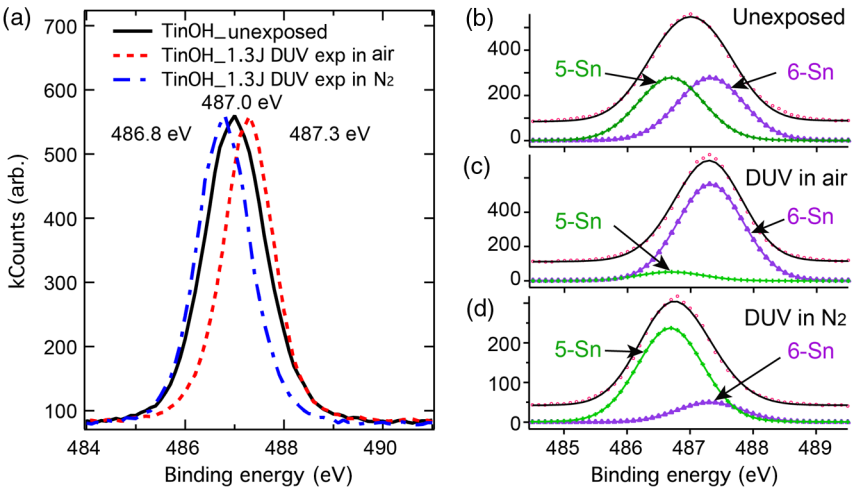

Fig. 3 Sn $3d_{5/2}$ core-level spectra for TinOH unexposed sample, TinOH DUV-exposed in air, and TinOH DUV-exposed in N_2. (a) Core-level spectra sharing the same scale on the ordinate axis. (b)–(d) Fits for each sample using the two-component model described in the text.

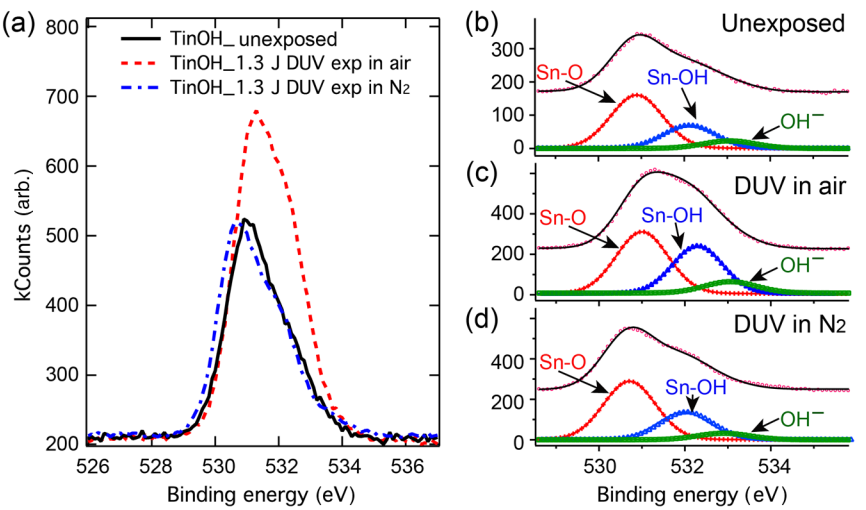

Fig. 4 The O 1s core-level spectra for TinOH unexposed sample, sample exposed in air, and sample exposed in N_2. (a) Core-level spectra sharing the same scale on the ordinate axis. (b)–(d) Least squares fits for each sample using the three-component model described in the text.

least squares fits to the data. As seen in Fig. 4(a), after DUV exposure in air, the O 1s peak shifted to higher binding energy and a considerably higher intensity, whereas the O 1s peak of the sample exposed under N_2 atmosphere shifted slightly to lower binding energies without a change of the intensity.[22]

There are three kinds of O atoms in the TinOH cage, as can be seen in Fig. 1. Three Voigt peaks are assumed in the modeling of the unexposed sample, each shown in Fig. 4(b). We assign the low-BE peak (red) to the oxygen atoms bridging three Sn atoms, the intermediate one (dark blue) to the oxygen in the OH groups bridging two Sn atoms, and the high-BE (light blue) to the O in the OH^- counterions. Similar to the Sn $3d_{5/2}$ fitting, we assume that the underlying spectral features in the spectra of the DUV-exposed samples are the same, i.e., their binding energy positions and linewidth parameters, whereas the intensities might be altered due to chemical conversion. Under these assumptions, the three spectra were fitted simultaneously to get a global optimum fit. The result is shown in Figs. 4(b)–4(d).

After the sample was exposed to DUV in air, the peaks of all three kinds of O increased in intensity. Because extensive oxidation has obviously taken place here, most probably resulting in a mixture of oxidation products, the simple approximation with three types of O is probably not fully valid, but again they do likely represent chemical environments close to those of the unexposed material. It is also possible that O_2^-, O_2^-, O_2^- would be chemisorbed on top of the photoresist.[24] For the sample exposed to DUV in N_2, on the other hand, no oxidation can take place, and the intensity of the three components almost stayed the same. The intensities of the peaks were converted into the number of oxygen atoms per molecule in the corresponding chemical state; the values are listed in Table 2, along with the extracted binding energy of the respective peak.

The C 1s photoelectron spectra were analyzed in the same way as their Sn 3d and O 1s counterparts. Figure 5(a) shows the data, normalized by the calculation from the overview spectra of the three samples. There is no clear energy shift observed in the main low-BE peak of the spectra after

Table 2 Relative numbers of three types of O atoms derived from O 1s spectra as well as extracted binding energies of the respective features (see Fig. 4).

Atom no.	Sn—O	Sn—OH	OH/CO	
Binding energy	530.7 eV	532.1 eV	533.0 eV	Total number
Expected	14	6	2	22
TinOH_unexposed	14	6	2	22
DUV exp air	16	13	3	32
DUV exp N_2	14	6	2	22

Table 3 Relative numbers of four types of C atoms derived from C 1s spectra (Fig. 5).

Atom no.	Sn—C	C—C	C—O	C=O	
Binding energy	284.9 eV	285.2 eV	286.1 eV	289.2 eV	Total number
Expected	12	36	0	0	48
TinOH unexposed	12	36	0	0	48
DUV exp air	3	9	5	1	18
DUV exp N_2	8	22	4	2	36

exposure, but the intensities and peak shape change significantly. In the unexposed sample, only two kinds of C atoms inside the tin-oxo cage can be distinguished from the spectra, being in Sn—C and C—C bonding configurations. After exposure, however, there is a shoulder observed near 286.1 eV and a new feature around 289.2 eV. These features likely arise from C 1s electron emission from C atoms with C—O and C=O bonds, respectively, as the increased BE indicates higher oxidation of some of the C atoms.[26] Thus, four Voigt peaks are used to describe the spectra of the DUV-exposed samples, the results of which are shown in Figs. 5(c)–5(d). The extracted concentration of the respective atomic type per molecule and the corresponding binding energies are listed in Table 3. The unexposed sample gives the ratio expected from the chemical structure. Furthermore, the C atom number in the C—C and Sn—C configurations from both samples exposed to DUV was decreased. At the same time, C in C—O and C=O binding motifs was increased slightly, which further demonstrated the oxidation during the DUV exposure. For the sample exposed in air, the C—O and C=O can be taken as a sign of oxidation on the carbon chain part, in agreement with the increasing of the O content. However, as we concluded from the overview spectra and Sn 3d, and O 1s spectra, there was no oxidation or O gain in the sample exposed to DUV in N_2. The increase of the C=O feature at 289.2 eV from the sample exposed in N_2 must, therefore, be because of a light-induced rearrangement within the tin-oxo cages. Although there is no extra O gained, the carbon chain might be cleaved at the Sn—C bond or C—C bond after which the product could further react with an oxygen atom in the cage to form C—O or C=O bonds.

Based on the analysis of the HAXPES data presented above, we propose reaction pathways of the DUV induced reaction, schematically shown in Fig. 6. According to quantum-chemical calculations, using density functional theory, the lowest electronically excited triplet state is of a $\sigma \rightarrow$ d type.[27] In this state, the Sn—C bond is easily broken to form two radicals. If present, oxygen and H_2O can directly react with the Sn radicals and increase the oxidation states of Sn atoms, which corresponds to the results shown in Fig. 3. The butyl radical could further donate a hydrogen atom or abstract one from neighbor cages to form butane or butene, volatile stable molecules that are readily released into a vacuum. A hydrogen atom could be abstracted from a butyl group and form a C-centered radical, which could further react and form side chain oxygenation products that may

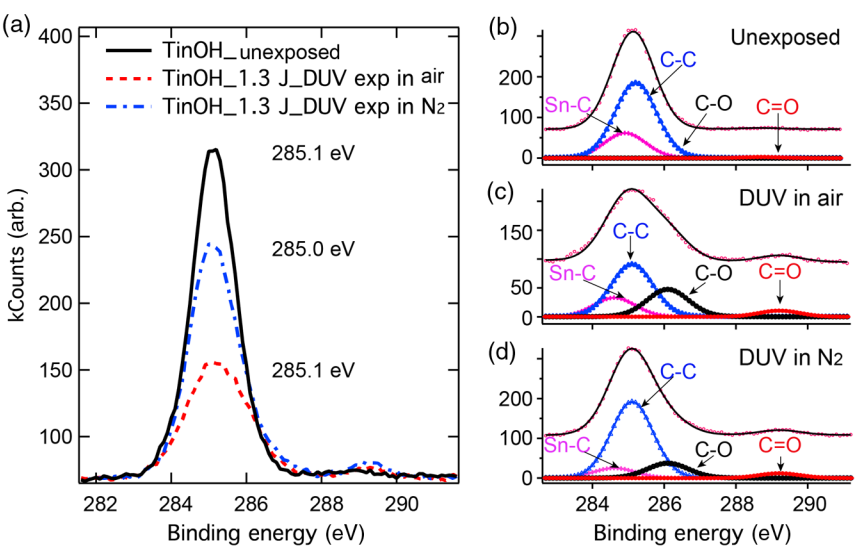

Fig. 5 (a) C 1s core-level spectra for TinOH unexposed sample, TinOH DUV-exposed in air, and TinOH DUV-exposed in N_2. (b)–(d) Fits for each sample using the four-component model described in the text.

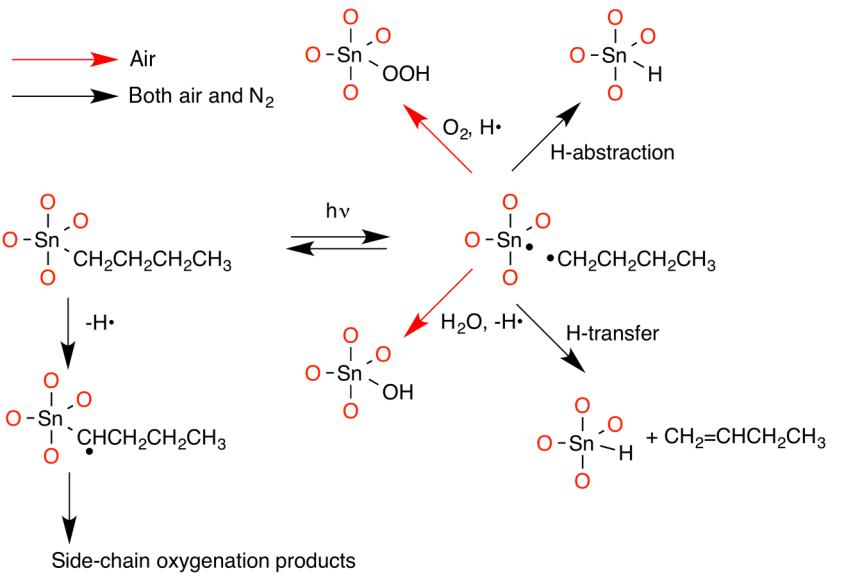

Fig. 6 Proposed photochemical reactions for TinOH exposed to DUV in air and N_2.

account for the 289.2-eV band in Fig. 5. For the sample exposed in N_2, the chance for the radicals to recombine is greater after the Sn—C bond cleavage occurs since there is no active molecule like O_2 or H_2O. That would explain why more C is lost in the sample exposed in air than in the sample exposed in N_2. The cleaved butyl radical could also react with the O inside the cage forming a C—O bond, corresponding to the C—O peaks in Figs. 5(c) and 5(d). Another possible reaction is the transfer of a hydrogen atom from the butyl radical to the Sn radical to form butane and a tin hydride. The formation of such an oxidation-sensitive but otherwise stable reaction product could be the explanation of our finding that the formation of insoluble material after exposure to EUV is enhanced by postexposure baking.[28]

4 Conclusion

HAXPES is demonstrated to be a powerful tool for analyzing the chemical changes upon DUV exposure in air and under N_2 in thin films of tin-oxo cages. Based on the detailed analysis of the presented HAXPES spectra, a mechanism of the photoreactions of TinOH films exposed to DUV in air or under N_2 could be proposed.

While the exposure conditions are very different from those in an EUV lithography tool, this study highlights the relevance of gas-phase/film interactions for the final photochemical product formation. In ongoing experiments, we further compare these results with the changes induced in solution-phase photochemistry of the tin cages in which products can be isolated and subjected to a wide range of chemical analysis techniques and with the results of EUV exposures of thin films at 13.5 nm.

Acknowledgments

Part of this work has been carried out at the Advanced Research Center for Nanolithography (ARCNL), a public-private partnership of the University of Amsterdam (UvA), the VU University Amsterdam (VU), the Netherlands Organization for Scientific Research (NWO), and the semiconductor equipment manufacturer ASML. We thank Michiel Hilbers (UvA) and Roberto Felix Duarte (BESSY-II), who provided expertise that greatly assisted the research. We thank HZB for the allocation of synchrotron radiation beam time. This work has been presented in part at the 2017 SPIE Advanced Lithography conference.[29]

References

1. L. Li et al., "Studying the mechanism of hybrid nanoparticle photoresists: effect of particle size on photopatterning," *Chem. Mater.* **27**(6), 5027–5031 (2015).
2. S. Chakrabarty et al., "Oxide nanoparticle EUV resists: toward understanding the mechanism of positive and negative tone patterning," *Proc. SPIE* **8679**, 867906 (2013).
3. S. Chakrabarty et al., "Increasing sensitivity of oxide nanoparticle photoresists," *Proc. SPIE* **9048**, 90481C (2014).
4. J. Stowers and D. A. Keszler, "High resolution, high sensitivity inorganic resists," *Microelectron. Eng.* **86**(4), 730–733 (2009).
5. T. S. Meyers et al., "Organometallic solution based high resolution patterning compositions and corresponding methods," US 2016/0116839 A1 (2015).
6. B. Cardineau et al., "Photolithographic properties of tin-oxo clusters using extreme ultraviolet light (13.5 nm)," *Microelectron. Eng.* **127**(7), 44–50 (2014).
7. M. Sortland et al., "Positive-tone EUV resists: complexes of platinum and palladium," *Proc. SPIE* **9422**, 942227 (2015).
8. R. Del Re et al., "Low-LER tin carboxylate photoresists using EUV," *Proc. SPIE* **9422**, 942221 (2015).
9. M. Trikeriotis et al., "A new inorganic EUV resist with high etch resistance," *Proc. SPIE* **8322**, 83220U (2012).
10. R. Fallica et al., "Dynamic absorption coefficients of chemically amplified resists and nonchemically amplified resists at extreme ultraviolet," *J. Micro. Nanolith. MEMS MOEMS* **15**, 033506 (2016).
11. T. Kozawa, "Lower limit of line edge roughness in high-dose exposure of chemically amplified extreme ultraviolet resists," *Jpn. J. Appl. Phys.* **51**, 06FC1 (2012).
12. F. Luo et al., "Helium ion beam lithography (HIBL) using HafSOx as resist," *Proc. SPIE* **9779**, 977928 (2016).
13. D. Fan and Y. Ekinci, "Photolithography reaches 6 nm half-pitch using EUV light," *Proc. SPIE* **9779**, 97761V (2016).
14. E. Hassanein et al., "Film quantum yields of ultrahigh PAG EUV photoresists," *Proc. SPIE* **69211**, 69211I (2008).
15. F. Banse et al., "Hydrolysis of monobutyltin trialkoxides synthesis and characterizations of $\{(BuSn)_{12}O_{14}(OH)_6\}(OH)_2$," *Inorg. Chem.* **34**, 6371–6379 (1995).
16. R. Fallica et al., "Absorption and exposure kinetics of photoresists at EUV," *Proc. SPIE* **10143**, 101430A (2017).
17. B. L. Henke, E. M. Gullikson, and J. C. Davis, "X-ray interactions: photoabsorption, scattering, transmission, and reflection at E = 50–30, 000 eV, Z = 1–92," *At. Data Nucl. Data Tables* **54**(2), 181–342 (1993).

18. N. Mårtensson, E. Sokolowski, and S. Svensson, "50 years anniversary of the discovery of the core level chemical shifts. The early years of photoelectron spectroscopy," *J. Electron. Spectrosc. Relat. Phenom.* **193**(7), 27–33 (2014).
19. M. Fondell et al., "An HAXPES study of Sn, SnS, SnO and SnO_2," *J. Electron. Spectrosc. Relat. Phenom.* **195**(5), 195–199 (2014).
20. F. Schaefers, M. Mertin, and M. Gorgoi, "KMC-1: a high resolution and high flux soft x-ray beamline at BESSY," *Rev. Sci. Instrum.* **78**(12), 123102 (2007).
21. M. P. Seah, "Post-1989 calibration energies for x-ray photoelectron spectrometers and the 1990 Josephson constant," *Surf. Interface Anal.* **14**(1), 488 (1989).
22. X. Xiao et al., "Enhanced formaldehyde sensing properties of SnO_2 nanorods coupled with Zn_2SnO_4," *RSC Adv.* **5**, 42628 (2015).
23. C. Liu et al., "Enhanced electrochemical stability of Sn-carbon nanotube nanocapsules as lithium-ion battery anode," *Electrochim. Acta* **144**, 376–382 (2014).
24. T. Kawabe et al., "Electronic states of chemisorbed oxygen species and their mutually related studies on SnO_2 thin film," *J. Phys. Chem. B* **105**, 4239–4244 (2001).
25. M. B. Trzhaskovskaya, V. I. Nefedov, and V. G. Yarzhemsky, "Photoelectron angular distribution parameters for elements Z = 1 to Z = 54 in the photoelectron energy range 100-5000 eV," *At. Data Nucl. Data Tables* **77**, 97–159 (2001).
26. C. M. Preuss et al., "A bioinspired light induced avenue for the design of patterned functional interfaces," *J. Mater. Chem. B* **2**, 36–40 (2014).
27. J. Haitjema et al., "Photoreactions of tin oxo cages, model EUV photoresists," *J. Photopolym. Sci. Technol.* **30**(1), 99–102 (2017).
28. J. Haitjema et al., "Extreme ultraviolet patterning of tin-oxo cages," *Proc. SPIE* **10143**, 1014325 (2017).
29. Y. Zhang et al., "Photochemical conversion of tin-oxo cage compounds studied using hard x-ray photoelectron spectroscopy," *Proc. SPIE* **10146**, 1014606 (2017).

Biographies for the authors are not available.